Printed in U.S.A.

71-GT-20

an ASME publication

$2.00 PER COPY
$1.00 TO ASME MEMBERS

Analytical and Experimental Studies of Two-Dimensional Flows in a Radial Bladed Impeller

R. S. BENSON
Professor of Mechanical Engineering

W. G. CARTWRIGHT
Lecturer in Mechanical Engineering

Dept. of Mechanical Engineering,
The University of Manchester
Institute of Science & Technology,
Manchester, England

M. J. HILL
Special Research Assistant

Dept. of Mechanical Engineering,
The University of Manchester
Institute of Science & Technology,
Manchester, England

The current state of a research program to study flows in radial turbomachines at both on- and off-design conditions is described. Numerical solutions of the flow within a rotating impeller are described based on potential theory using a direct method of solution instead of by relaxation. The experimental apparatus comprising a rotating cascade rig is described. The rig consisted essentially of a rotor mounted horizontally in an open circular water tank. An external pipe system enabled the water to be circulated for either radial inflow or radial outflow. The rotor speed could be varied up to 300 rpm. A variety of perspex shrouded rotor geometries up to a maximum diameter of 3 ft 6 in could be tested. Flow visualization by means of polystyrene particles could be observed by a camera mounted above the rotor on its axis and driven at the same angular speed. A 12-channel electronic flash unit enabled the particle velocity and directions to be photographed. As an alternative to the flow visualization system, a bank of manometers, could be mounted above the rotor and driven at the same rotational speed, i.e., with no relative movement. Static pressure measurements could be taken on the blade faces and within the rotor passages. A comparison is made of the experimental and analytical results obtained for one straight vaned, constant area rotor.

Contributed by the Gas Turbine Division of The American Society of Mechanical Engineers for presentation at the Gas Turbine Conference & Products Show, Houston, Texas, March 28-April 1, 1971. Manuscript received at ASME Headquarters, November 27, 1970.

Copies will be available until January 1, 1972.

THE AMERICAN SOCIETY OF MECHANICAL ENGINEERS, UNITED ENGINEERING CENTER, 345 EAST 47th STREET, NEW YORK, N.Y. 10017

Analytical and Experimental Studies of Two-Dimensional Flows in a Radial Bladed Impeller

R. S. BENSON **W. G. CARTWRIGHT** **M. J. HILL**

INTRODUCTION

Considerable attention has been given in recent years to the quantitative analysis of flows within turbomachinery blading. The major emphasis has been on axial machinery, where it is possible to assess the results by experiments on stationary blade cascades. The problem is relatively more difficult in radial and mixed flow machines where changes in centripetal acceleration along streamlines are large and static cascade testing is not satisfactory. In the past five years, comprehensive studies on flows in radial machines have been carried out in the Thermodynamics and Fluid Mechanics laboratories at the University of Manchester Institute of Science and Technology. This work has been sponsored by the Science Research Council and a number of industrial firms. From

NOMENCLATURE

$\underline{A}$ = band matrix used in direct method of solution

a_T = area at impeller tip

C_o = stagnation speed of sound upstream of impeller

h = passage height

h_T = passage height at impeller tip

H = passage height ratio h/h_T

M_T = tip Mach number $r_T \omega / C_o$

nb = number of blades

p = static pressure

P = constant $Q^2(\rho/\rho_o)^2$ at a grid point

p' = pressure recorded at reference pressure tapping

q = relative velocity

Q = relative velocity ratio, q/C_o

r = radius from axis of rotation

r_T = impeller tip radius

R = radius ratio, r/r_T

s = radial step-length of finite difference molecule (Fig.2)

t = theta step-length of finite difference molecule (Fig.2)

U = blade speed

V = absolute velocity

W_T = total weight flow through impeller passage

y = right-hand side vector used in direct method of solution

α = angle between meridional stream surface and axis of rotation

κ = ratio of specific heats

λ = whirl ratio, $R(RM_T + Q_\theta)$

ρ = density

ϕ = flow coefficient, V_r/U_2

ψ = stream function

ψ_n = stream function value of the total flow through the impeller passage, $2\pi W_T/(nb.\rho_o\, a_T\, C_o)$

$\underline{\psi}$ = vector of stream function values obtained from $\underline{A}\,\underline{\psi} = \underline{y}$

θ = relative angular co-ordinate

ω = rotational speed

Subscripts

M = meridional component
k = constants evaluated at grid-point k
o = obsolute stagnation condition
p = constants evaluated at grid-point p
q = constants evaluated at grid-point q
r = radial component
R = partial derivative with respect to radius ratio R in equation numbers (1), (3), (4), (5), (8), (9)
R = radial component
RR = second partial derivative with respect to radius ratio R
u = upstream property
θ = partial derivative with respect to θ in equation numbers (1), (3), (4), (5), (8), (9)
θ = theta component
$\theta\theta$ = second partial derivative with respect to θ
2 = impeller blade inlet station

Superscripts

- Mass mean value

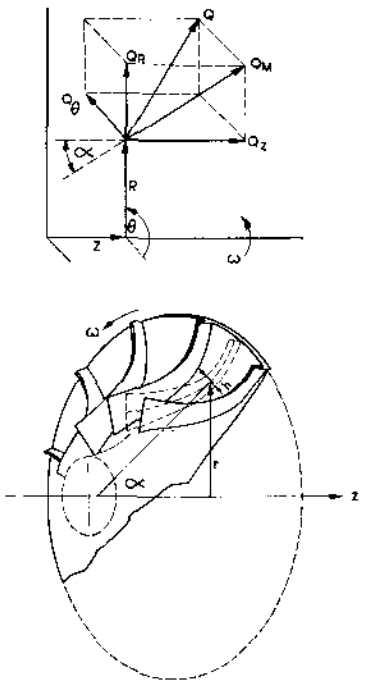

Fig.1 Coordinate system relative to blades. Centerline of flow passage generates a surface of revolution

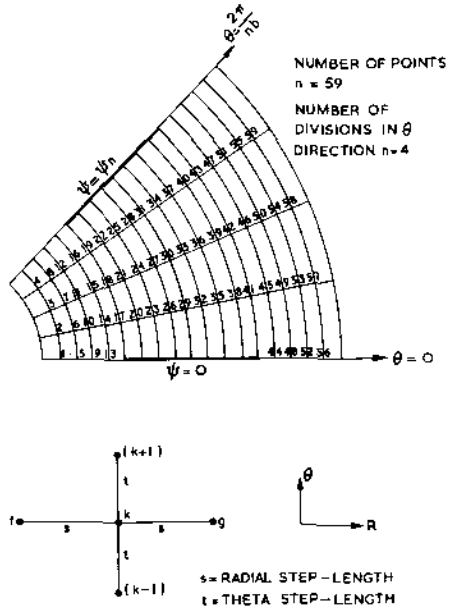

Fig.2 Numerical solution in blade-to-blade plane

time to time, results of this work have been reported (1-8).[1] In this paper, some recent results are described.

The analytical work has been mainly concentrated on extending the streamline curvature techniques of Katsanis (8-10) and the direct solution of the fluid flow equations similar to Stanitz (11) methods. The Katsanis methods have been refined and improved, and it is now possible to study flows in passages which may be supersonic. This work is not reviewed in this paper. Stanitz's approach to a numerical solution of the two-dimensional irrotational equations has been reassessed, and a new numerical solution has been developed which is both faster than the relaxation techniques used by Stanitz and can cover the whole flow region from the upstream to downstream boundaries beyond the rotor in either direction. This method will be described in this paper.

Work is also being pursued in the Department on boundary layers in rotating systems and full field solutions of the viscous turbulent equations of motion.

In conjunction with the analytical work, an extensive experimental program is being carried out including turbine testing. In this paper, a special radial cascade rig is described. This rig was developed to test the analytical solutions. The paper will discuss some results of tests on a straight-vaned constant area impeller running as a radial inflow turbine. Comparison will be made between the potential solutions and experimental results.

ANALYTICAL PROCEDURE

From consideration of continuity, absolute irrotational motion, and energy, the steady two-dimensional inviscid flow through a turbomachine can be represented for the coordinate system shown in Fig.1 by:

$$\sin\alpha\ \psi_{RR} + \frac{\psi_{\theta\theta}}{R^2\sin\alpha} - \frac{\psi_\theta}{R^2\rho/\rho_o\sin\alpha}\left(\frac{\rho}{\rho_o}\right)_\theta + \frac{\psi_R}{R}\left[(R\sin\alpha)_R - \frac{R\sin\alpha}{\rho/\rho_o}\left(\frac{\rho}{\rho_o}\right)_R - \frac{R\sin\alpha}{H}H_R\right] = 2M_T^2\frac{\rho}{\rho_o} \quad (1)$$

$$\frac{\rho}{\rho_o} = \left\{1 + \frac{\kappa-1}{2}\left\{(RM_T)^2 - Q^2 - 2M_T\lambda_u\right\}\right\}^{\frac{1}{\kappa-1}} \quad (2)$$

$$Q\frac{\rho}{\rho_o} = \left[\left(\frac{\sin\alpha\psi_R}{H}\right)^2 + \left(\frac{\psi_\theta}{HR}\right)^2\right]^{\frac{1}{2}} \quad (3)$$

Combining these three equations and transferring all density terms to the right-hand side, we obtain the expression

$$\sin\alpha\ \psi_{RR} + \frac{\psi_{\theta\theta}}{R^2\sin\alpha} + \frac{\psi_R}{R}\left[(R\sin\alpha)_R - \frac{R\sin\alpha}{H}H_R\right] = 2M_T^2\frac{\rho}{\rho_o} + \frac{\psi_\theta}{R^2\rho/\rho_o\sin\alpha}\left(\frac{\rho}{\rho_o}\right)_\theta + \frac{\psi_R\sin\alpha}{\rho/\rho_o}\left(\frac{\rho}{\rho_o}\right)_R \quad (4)$$

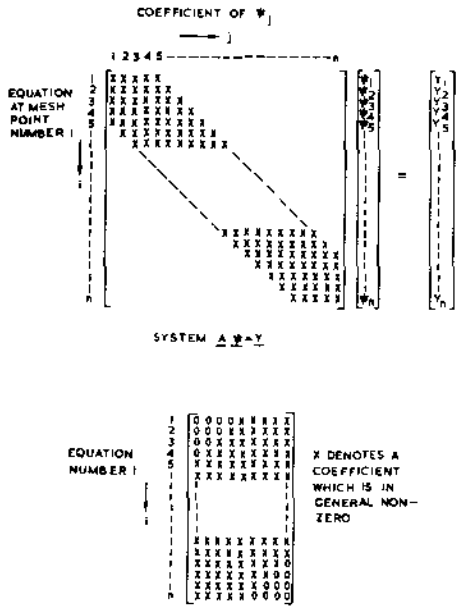

Fig.3 Computer storage of band matrix, $\underline{A}$

This can be expressed in the form

$$A\,\psi_{RR} + B\,\psi_{\theta\theta} + C\,\psi_R = D \qquad (5)$$

where

$$A = \sin\alpha \qquad (6)$$

$$B = \frac{1}{R^2\sin\alpha} \qquad (7)$$

$$C = \frac{1}{R}\left[(R\sin\alpha)_R - \frac{R\sin\alpha\, H_R}{H}\right] \qquad (8)$$

$$D = 2M_T^2 H\frac{\rho}{\rho_o} + \frac{\psi_\theta(\rho/\rho_o)_\theta}{R^2(\rho/\rho_o)\sin\alpha} + \frac{\psi_R\sin\alpha(\rho/\rho_o)_R}{\rho/\rho_o} \qquad (9)$$

Numerical Method of Solution

The solution of equation (5) is computed using a "direct" method instead of relaxation. The region of solution, i.e., the rotor passage together with upstream and downstream regions, is covered with an orthogonal polar grid (Fig.2) and the finite difference equations set up at each numbered grid point. A system of equations is then obtained which may be written in the form

$$\underline{A}\,\underline{\psi} = \underline{Y}$$

where $\underline{A}$ is a band matrix, $\underline{y}$ is a vector, and $\underline{\psi}$ is the required solution at the grid points.

Using the conventional finite-difference approximations, the general finite difference equation at a grid point k is given by

$$E_k\psi_f + F_k\psi_{k-1} + G_k\psi_k + H_k\psi_{k+1} + I_k\psi_g = J_k \qquad (10)$$

where

$$E = t^2(2A - sC) \qquad (11)$$

$$F = 2B\,s^2 \qquad (12)$$

$$G = -4\,(At^2 + Bs^2) \qquad (13)$$

$$H = 2Bs^2 \qquad (14)$$

$$I = t^2(2A + sC) \qquad (15)$$

$$J = 2D\,s^2t^2 \qquad (16)$$

At each of the numbered mesh points, the constants (E, F, G, H, I, and J) can be evaluated and the finite difference equation formed at the mesh point. At mesh points adjacent to the boundary of the region of solution, some of the ψ_f, ψ_g, ψ_{k-1}, and ψ_{k+1} values will be known. These are transferred to the right-hand side of equation (10). Periodicity considerations enable ψ_{k+1} to be determined for mesh points such as 4 and 8 of Fig.2, also the ψ_{k-1} values for points such as 1 and 5. The coefficients of the unknown ψ values for the set of finite difference equations for the system form the matrix $\underline{A}$, thus

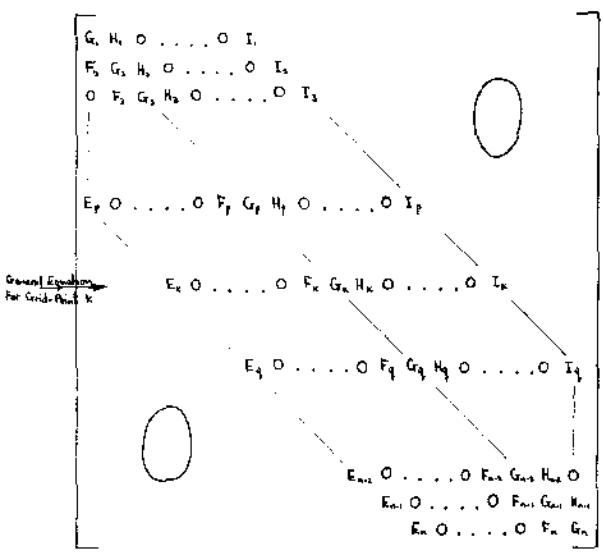

The known right-hand side terms for the set of finite-difference equations form the vector $\underline{Y}$. The set of finite difference equations can then be expressed in the matrix form:

$$\underline{A}\,\underline{\psi} = \underline{Y} \qquad (17)$$

where $\underline{A}$ is an n x n matrix of band width 2m+1, where n is the total number of numbered mesh points and m is the number of divisions in the θ

direction. $\underline{\psi}$ and $\underline{y}$ are n x 1 column vectors.

In the computer solution of equation (17), only the band elements of matrix $\underline{A}$ are stored (Fig.3). It will be seen that $\underline{A}$ is only dependent on the rotor geometry and the number of grid points. Thus, $\underline{A}$ is set up only once and the system of equations solved for each new right-hand side vector, $\underline{y}$.

The numerical solution of equation (17) is, by Gaussian elimination, using the Thomas Algorithm (12). For incompressible flow, there is one unique value for the vector, $\underline{y}$, and a solution of equation (17) is straightforward. For compressible flow, the density ratio, ρ/ρ_o, varies with each successive iteration at the grid points until convergence. The normal procedure is to evaluate the constant, $P = (Q\ \rho/\rho_o)^2$, at each grid point, from equation (3), and then by using equation (2), the density ratio is a root of the expression

$$f\left(\frac{\rho}{\rho_o}\right) = \left(\frac{\rho}{\rho_o}\right)^{\kappa-1} - \left[1 + \frac{\kappa-1}{2}\left\{(RM_T)^2 - \frac{P}{(\rho/\rho_o)^2} - 2M_T\lambda_u\right\}\right] \quad (18)$$

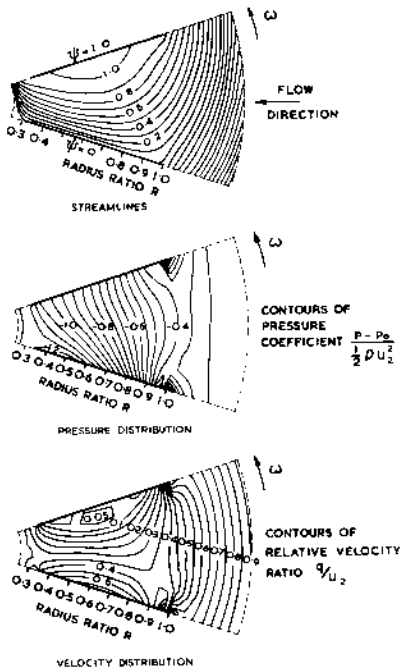

Fig.4 Computed results for rotor described in experimental rig

This expression has either two real roots or no real roots. The larger root is associated with subsonic flow and the smaller root with supersonic flow. Differentiating equation (18) and equating to zero, we obtain a function, $f(P^{1/\kappa+1})$. This corresponds to the minimum value of the function, $f(\rho/\rho_o)$, where $\rho/\rho_o = P^{1/\kappa+1}$. When $f(P^{1/\kappa+1}) \leq 0$, then $f(\rho/\rho_o)$ has two real roots and the required root is found by an iterative procedure, such as the Newton-Raphson method. When $f(P^{1/\kappa+1}) > 0$, then $f(\rho/\rho_o)$ has no real roots. This may occur in the first few iterations. In these cases, the density ratio is taken as the minimum value of $\rho/\rho_o = P^{1/\kappa+1}$.

An alternative method, which is superior to the foregoing, is to use the previous value of the density ratio in equation (3) to determine Q, then with this value of Q determine the new approximate value of the density ratio from equation (2). Experience has shown that the approximation to the density ratio converges as the whole problem converges. This new technique has three distinct advantages over the first method:

1 For high Mach number solutions, the solution stabilizes very rapidly and convergence is obtained in considerably fewer iterations than the previous methods. Indeed, solutions have now been obtained which could not converge with the first method.

2 Computing time has been reduced.

3 Since the new method does not require a prior knowledge of which grid points in the final solution will be subsonic or supersonic, the method may enable a transonic solution to be obtained.

Boundary Conditions

The first solution is obtained with approximate boundary conditions corresponding to one-dimensional calculations. These boundary conditions are then progressively adjusted and the solution repeated until the required inlet and outlet conditions are obtained. The outlet condition usually applied is that of Joukowski, requiring the rear stagnation point to occur at the blade trailing edge. At inlet there are two alternatives, either the rotor inlet whirl, λ_u, may be specified or the "on-design" condition may be required, i.e., the front stagnation point occurring at the blade leading edge.

The techniques outlined in the foregoing have been, and are being, applied to various rotor configurations. In this paper, a comparison will be made between the flow predictions and measurements for a straight-vaned, constant area rotor with an incompressible fluid. Typical computed results direct from graphical output for the streamlines, pressure, and velocity distribution for the rotor described in the experimental rig are shown in Fig.4. (The discontinuities are due to the graph plotter.)

EXPERIMENTAL INVESTIGATION

As part of the study of flows in radial machinery, an experimental facility was con-

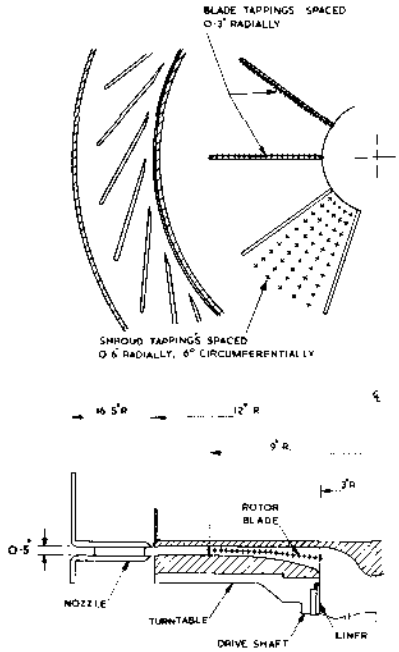

Fig.5 Arrangement of rotor and nozzle showing location of static pressure tappings

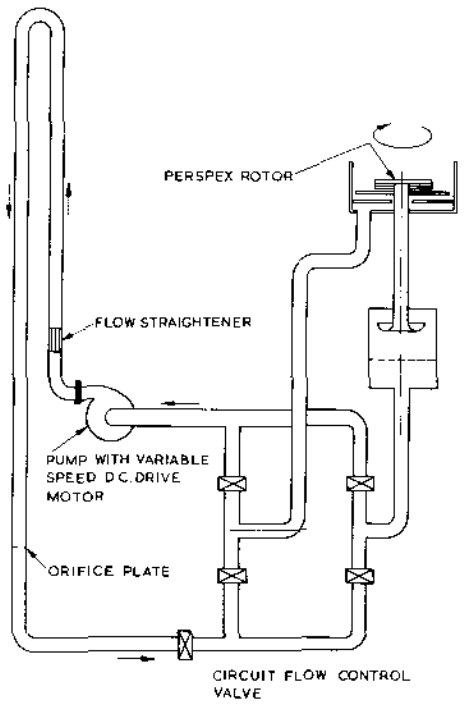

Fig.6 Diagrammatic layout of water circuit

structed with the object of determining the actual flow distribution within a rotating impeller. The working fluid was water. A knowledge of the real flow permits:

1 An assessment of the various numerical techniques for calculating flows on and off design to be made
2 An evaluation of the possible refinements to be made to the numerical techniques to approximate closer to the real flow
3 The provision of data on the gross effects of fluid friction to be obtained.

The rig was designed to examine radial inflow or outflow. Provision was made to measure the static pressure distribution within the blade passage, as well as on the blade faces. Flow visualization techniques were incorporated to obtain a qualitative and quantitative measurement of the velocity and streamline patterns within the rotor passages. In a previous paper (5), some results were presented for the pressure distribution on the blade faces; in this paper, some results are presented for the pressure and relative velocity distributions within the blade passage in a simple geometry radial bladed rotor operating under turbine-type inflow conditions at a positive incidence angle.

Test Rig

The rotor under test was mounted on a horizontal turntable, the hollow drive shaft of which served as a duct for the flow of water to or from the rotor. In the tests described in this paper, the rotor had ten flat radial blades the height of which varied with the radius so as to give a constant flow area. Top and bottom shroud disks were extended radially beyond the blades to preserve the two-dimensional nature of the flow at the blade tip. Fig.5 shows the principal dimensions of the rotor.

An open-topped circular tank surrounding the rotor was provided with a duct connection to permit external recirculation of the flow via a metering section, Fig.6. The rotor could be operated either with outward flow, as in a centrifugal pump, or with inward flow, as in a turbine. In the former case, water rose vertically upward through the drive shaft and then outward through the rotor discharging into the tank. The water was recirculated by the external pipe work back to the "eye" of the rotor. The pressure rise required to achieve circulation was provided by a pump in the external circuit. A variable speed drive to the pump minimized the amount of throttling needed to obtain flow rates other than the maximum. This minimized the water temperature rise with time and thus the viscosity variation. The external system was arranged to maintain the same flow direction through the pump and metering section for both inflow and outflow in the rotor. At all flows and rotor speeds so far investigated, the power absorbed by the large diameter seals surrounding the hollow shaft of the test rotor has been greater than the power developed by the rotor when operating as a turbine. The new power input to the rotor was provided by a variable

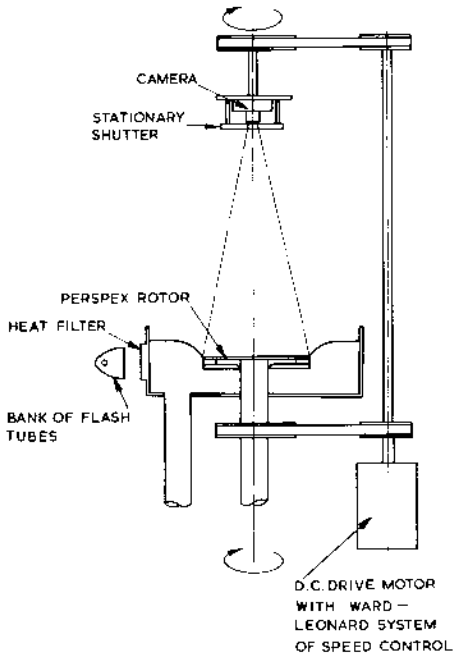

Fig.7 Diagrammatic layout of test rig

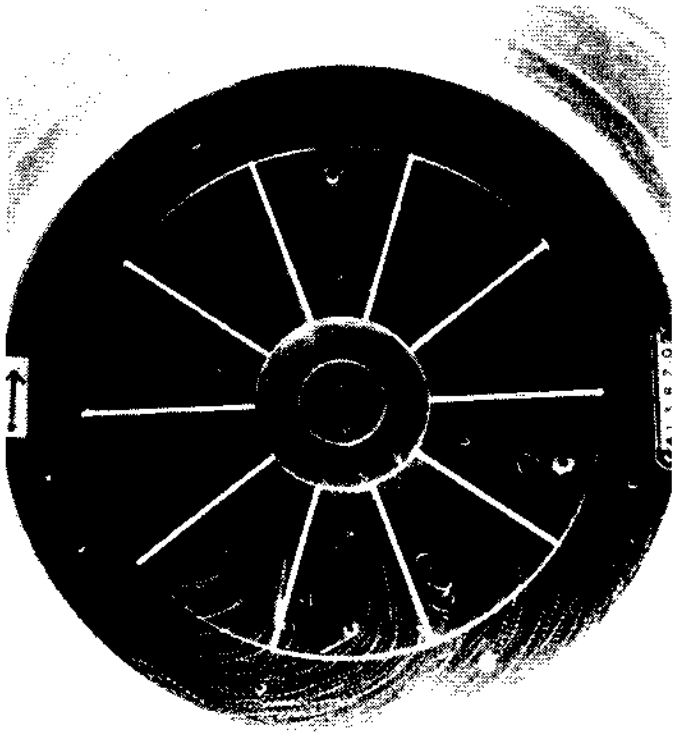

Fig.8 Flow relative to rotor

speed d-c motor with Ward Leonard control. The drive to the rotor was also linked to a second shaft, co-axial with the rotor, carrying a camera, Fig.7. The camera rotated at the same angular speed as the rotor and enabled the flow relative to the blading to be recorded. Flow visualization was made possible by polystyrene tracer particles, approximately 0.03-in. dia and having a specific gravity within the range 1.00 to 1.01. The technique used was similar to that of Young (13) and Simpson and Cinnamond (14). In the test rig, the particles were illuminated by a light source adjacent to a window in the side of the circular tank surrounding the water. The side-lighting arrangement had the advantage of illuminating the tracer beads but not the background, thus providing the maximum contrast as viewed by the camera. The disadvantage of sidelighting was that the stationary blading surrounding the rotor must be transparent. A particularly intense light source was found to be necessary. A special illumination system was developed. This consisted of a bank of electronic flash tubes. The tubes, each rated at 100 Joules, were triggered in rapid succession by a magnetic pickup receiving a signal from gear teeth in the rotor drive. The resulting flashes were, therefore, at a frequency proportional to the rotor speed. The flash sequence was recorded by the camera on a single exposure, which showed the positions taken by the flow visualization particles at equal intervals of time. Fig.8 is a typical example of one exposure showing a number of trajectories followed by particles present at the time of exposure. For this case, the rotor

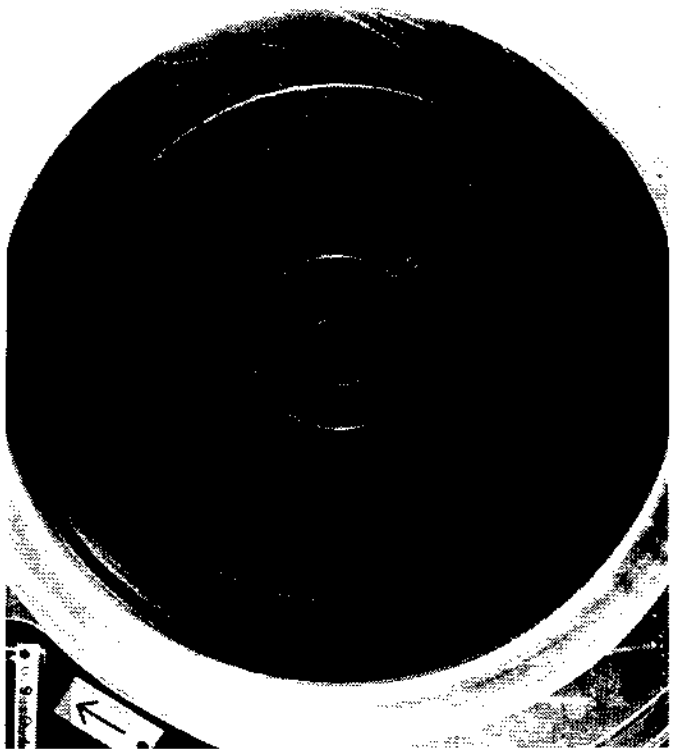

Fig.9 Absolute flow

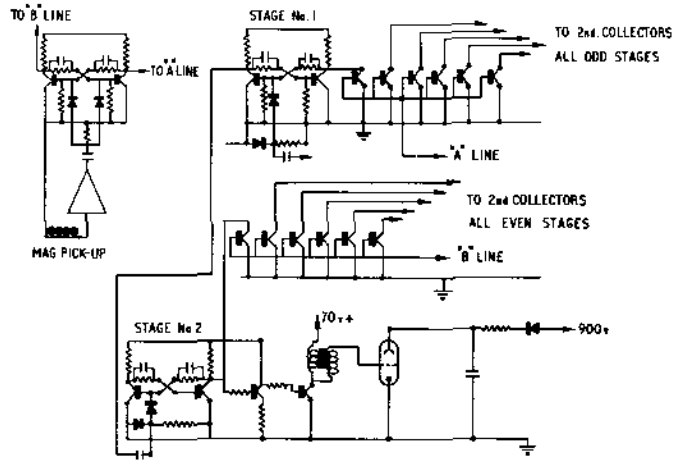

Fig.10 Electronic flash circuit

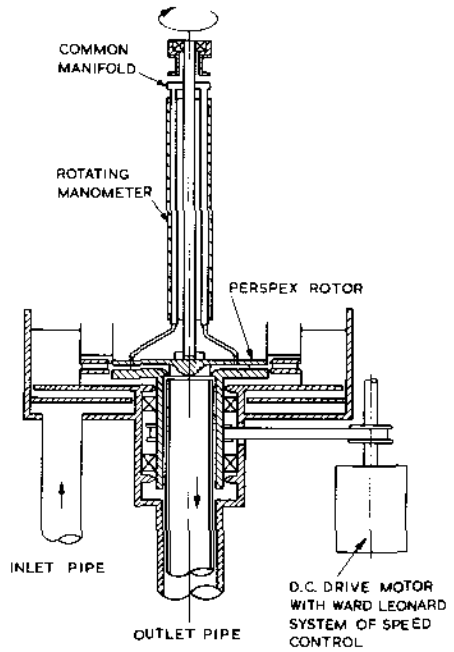

Fig.11 Diagrammatic layout of rotating manometer

was acting as a turbine under inflow conditions. The direction of rotation was clockwise. Fig.9 shows an exposure taken for the same flow conditions as Fig.8, but with the camera drive disconnected. Fig. 9 is, therefore, a record of the absolute, rather than the relative flow.

The evaluation of the velocity distribution from records, such as those shown in Figs.8 and 9, will be discussed in the following. At this point, it is interesting to note that the relative flows show streamline configurations qualitatively similar to the potential flow calculations shown in Fig.4. The intersection of the streamlines in absolute flow (Fig.9), most marked at the blade mid-radius position, are due to the considerable circumferential variation in the radial component of velocity across the blade passage. Particles close to the leading blade face (Fig.8) have a large inward (radial) velocity component, while particles in the eddy at the trailing blade face have a small outward (radial) velocity. The fan of radial lines shown in Fig.9 corresponds to a mark along one blade edge, designed to show if any flash tube failed to fire.

The circuit used to trigger the flash tubes is shown in Fig.10. The output from the magnetic pickup was fed into a conventional bi-stable multi-vibrator circuit, which alternatively provided a pulse for each of two collectors, connected respectively to the "A" line and the "B" line. When the "A" line received a pulse, this would switch off any stage which happened to be on. The action of switching off this stage produced a pulse at its "on" position which, since this was coupled to the input of the next stage in the chain, would switch it on. The next pulse would be in the "B" line and would produce the same sequence. The process would be repeated at the speed of the signal received from the magnetic pickup. The output pulses, taken from the "on" collectors of each stage, were fed first to an emitter follower stage to increase the power of the switching pulses and then to a power output stage, the collector load of which was the flash tube. Pilot lights and storage oscilloscopes were used to indicate whether all tubes fired and to record those which fail to do so. Additional circuitry was also developed to double or quadruple the time interval between flashes, in order to "space" the particles under certain flow conditions.

Static pressure measurements in the blade passage were made on the upper shroud surface and the blade surfaces. For these tests, the camera was replaced by a cylindrical cluster of eight manometer tubes. The manometer assembly was also driven so that there was no relative movement to the rotor. Fig.11 shows a diagram of the arrangement. A similar method of recording pressures in rotating machinery has been used by Acosta and Bowerman (15). In normal operation, all the manometer tubes were connected at their upper ends to a common manifold. The lower end of each tube was coupled to a pressure tapping in the top shroud of the rotor. Water was drawn into the manometer tubes by reducing the air pressure in the manifold below atmospheric pressure. One manometer tube was permanently connected to a reference pressure tapping point at the periphery of the top shroud. The other manometers recorded the pressure difference from this reference pressure. The shroud pressure tappings are shown in Fig.5. These were distributed between two of the blades. The tappings were equally spaced circumferentially at

each of ten radial stations. The pressures at one particular radius were recorded simultaneously with the reference pressure on each test run. An allowance was made for the difference in the pitch circle radii of the static pressure tappings and the manometer. To record the pressure distribution in a blade passage for one test condition, ten runs were required. The manifold pressure was normally different for each run. In order to relate the pressures recorded on different runs with one another and with the pressure level of the water outside the rotor, it was necessary to calibrate the reading at the reference pressure tapping, in relation to the absolute stagnation pressure of the fluid at the rotor tip. This was carried out in a separate series of tests. In these tests, two of the rotating manometer tubes were connected together at their lower ends. One of these tubes was disconnected from the manifold and vented to atmosphere at its upper end. With this configuration, the pair of tubes acted as a simple U-tube for measuring the gage pressure in the manifold. It was then possible to deduce the actual pressures at the reference tapping. The difference between the total pressure of the incoming liquid, p_o, and the reference pressure, p', when expressed as a coefficient, $p_o - p'/1/2\rho U_2^2$, was found to vary as the square of the flow coefficient, ϕ = mean radial velocity in rotor passage/ rotor tip speed = V_r/U_2. For the geometry of the rotor and guide vanes shown in Fig.5, the relationship was $p_o - p'/1/2\rho U_2^2 = 2.77\phi^2$.

EXPERIMENTAL RESULTS

The rotor used in the tests to be discussed here is shown in Fig.5. The nozzle ring contained 31 vanes. The exit angle was 73 deg. The radius of the nozzle trailing edge was 12.5 in. The shrouds at the top and bottom of the nozzle vanes were extended beyond the trailing edge to give a radial clearance of 0.02 in. with the rotor shrouds (Fig.5). This geometry gave a wide vortex space, measuring 3.5 in. radially between the nozzle exit and the rotor inlet.

The tests to be discussed were carried out at a rotor speed in the range 160 to 200 rpm with a flow coefficient, ϕ = -0.25 (the negative sign indicating radial inflow). The mean radial velocity, V_r, was taken as the volume flow rate divided by the flow area at the blade tip. Under these conditions, the absolute fluid flow angle in the vortex space between the nozzle and the rotor was 67.3 deg. This gave a mean angle of incidence at the rotor inlet radius of 29.2 deg. Care must be exercised in defining the angle of incidence in flows where there is an appreciable blade to blade variation of flow angle. The large annular clearance upstream of the rotor blading created the situation of an upstream "boundary condition" well removed from the blading, as was assumed in the potential flow calculations (Fig.4). These calculations showed that the local angle of incidence at the blade could be significantly different from the angle which the bulk flow made with the blade. From the potential flow calculation (Fig.4), zero incidence local to the blade tip was achieved when the mean tangential component of the absolute fluid velocity, $\bar{V}_{\theta 2}$, was 0.814 U_2. The velocity triangle at the blade tip is shown in Fig.12. When the absolute flow angle was 67.3 deg and $\bar{V}_{\theta 2}$ = 0.814 U_2, the mean relative flow angle was 28.8 deg. The flow coefficient, $\phi = V_{r2}/U_2 = 0.25$, gave a mean relative flow angle of 58.0 deg. On this basis, the mean angle of incidence was 58.0 deg - 28.8 deg = 29.2 deg.

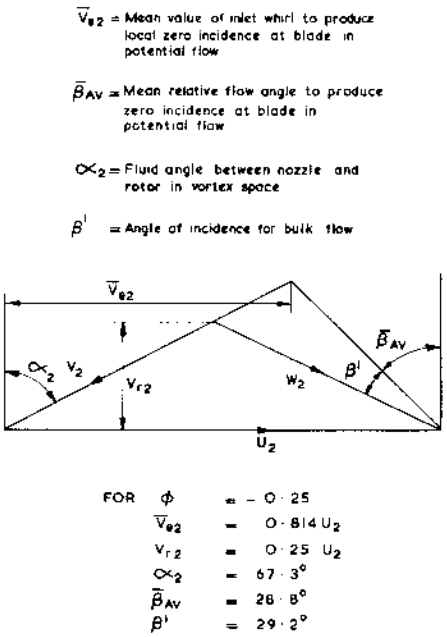

Fig.12 Velocity triangle at rotor inlet

Flow Visualization Results

In order to obtain a quantitative picture of the velocity distribution over the whole blade passage, a large number of photographs similar to Fig.8 must be analyzed until trajectories have been identified which pass through all regions of the flow field. Enlarged photographs of the trajectories were processed on an X-Y reader and the coordinates stored on punched paper tape. The nature of the triggering circuit for the electronic flash unit ensured that, regardless of rotor speed, the rotor moved through a fixed angle between successive flashes. The spacing of the dots on the relative flow photographs (Fig.8) could, therefore, be readily expressed as the dimensionless relative velocity ratio, q/U_2. Fig.13

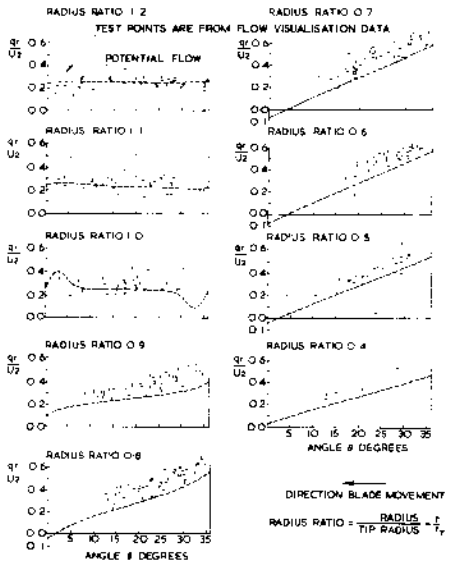

Fig.13 Relative velocity distribution. Comparison of flow visualization data with potential flow

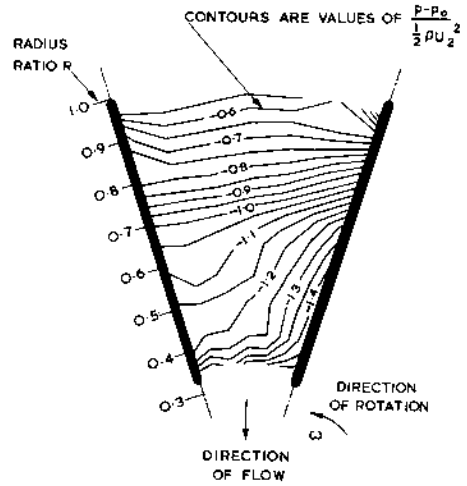

Fig.14 Measured static pressure distribution between blades

shows the results of an analysis of a large number of records of the type shown in Fig.8. The radial component of the relative velocity (q_r/U_2) is shown as a function of θ at a number of radius ratios. These are the raw results, obtained by direct analysis of the photographs. The scatter is due to the variability of the flow. This can be seen by visual inspection of a typical photograph in Fig.8. On the same graph (Fig.13), the potential flow solution for the velocity distribution, from Fig.4, is shown. A discussion of these results follows later.

Pressure Distribution Results

The results of the survey of the static pressure distribution on the rotor upper shroud are shown in Fig.14. The test results at the locations shown in Fig.5 were processed in a computer to give lines of constant pressure coefficients, $p-p_o/1/2\rho U_2$. The comparative potential solution is shown in Fig.4.

DISCUSSION OF RESULTS

Flow Visualization

The variability of flow in the rotor passage may be due to a number of possible causes. These may be:

1 Nonuniform flow entering the rotor resulting from nozzle blade wakes disturbances upstream of the rotor or imperfect nozzle spacing
2 Three-dimensional flow within the blade passage
3 Geometric dissimilarities between the rotor blades and blade spacing
4 Large-scale turbulence within the rotor.

All the foregoing causes may or may not be present. Notwithstanding these effects, some general trends are clearly present. Outside the rotor, radius ratio greater than 1.0, the general trend in the experimental results agrees with the potential solution. As we pass into the rotor, the experimental points tend to drift upward from the potential solution. The "slope" of the results follow the potential solutions. Since the blade height varies with radius in such a manner as to maintain a constant flow area, the average value of q_r should be the same at all radii, and the mean value of q_r/U_2 should be equal to the flow coefficient -0.25 at each radius. The potential flow velocity distribution satisfies this condition. The experimental results appear to indicate a progressively increasing value of q_r with decrease in radius. Some possible explanation for these effects may be:

1 Boundary-layer effects reducing the effective flow area
2 Increase in the eddy region. The photographic analytical technique does not differentiate between flow directions.
3 The low particle speeds, particularly in the eddy region, did not give a readable trace and were, therefore, missing from the photographs.

The possible explanation is probably a combination of all these effects.

Pressure Distribution

A comparison of the experimental results (Fig.4) and the potential results (Fig.4) show that the recorded pressure coefficients are lower than the ideal values by an amount varying from

0.3 to 0.2. Pressure gradients along the trailing blade face (at the right-hand side of the figure) are predicted reasonably well by potential flow, but there is some discrepancy at the leading blade face. The lower observed pressures are compatible not only with what might be anticipated from fluid friction considerations, but also from the observed higher relative velocities in Fig.13.

General Discussion

The work discussed in this paper is a progress report on the studies in radial turbomachinery currently being pursued at the University of Manchester Institute of Science and Technology. At this stage no definite conclusions can be drawn. The results reported here and in a previous paper (5) indicate that the potential solutions of the flow in the radial rotor passages give a good qualitative picture and fairly reasonable quantitative results. It is quite clear that boundary-layer effects are significant. It follows, therefore, that for reliable quantitative results, some method of including the fluid friction in the analytical techniques is required. Three methods, varying in complexity, may be used. These are:

1 The introduction of a loss term in the basic equations either as a loss in stagnation pressure or an increase in entropy. This method has been described by Katsanis (8-10) and applied by Benson, Cartwright, and Woollatt (4) to a small radial turbine. It should not be difficult to include this in the methods used in this paper.

2 The computation of the boundary-layer growth on the blade passage walls. An attempt has been made to apply this technique with some success, provided separation does not occur in the passage. In the calculation procedures used so far, separation appears to occur with normal flow rates even at zero incidence, but not in all cases. Some qualitative assessment, however, may be made particularly with regard to fluid friction losses and blockage. The latter may be included in the rotor geometry and the former in some loss term as described in the foregoing.

3 The solution of the full fluid flow equations with viscosity and turbulence terms. This is the most complex of all the methods and depends to a great extent on the size of the computer facility. Preliminary work is proceeding on these lines, and some results may be available at the presentation of the paper.

Despite the lack of definitive quantitative information from the potential solution, the methods can still be used to assess a design. For example, the actual performance of a turbomachine may be well documented. Running conditions may be known at which, for example, the flow separates at a certain point, and other conditions may be known at which separation does not occur. The flow at the two sets of conditions could be analyzed by the potential methods. By comparing pressure gradients, as indicated by the frictionless calculations, experience could be gained in the limiting calculated value of this parameter which proves to be acceptable in the real flow. Here, of course, it is important to have a reliable potential solution. The methods discussed in this paper offer such a technique. The accumulation of experimental work on the rig described in this paper will enable the introduction of suitable modifying factors to be introduced into the analytical method which will enable a closer quantitative prediction. This work is currently being pursued.

CONCLUSIONS

The paper reviewed current work on flow in radial turbomachines being carried out in the University of Manchester Institute of Science and Technology. A numerical solution for potential flow in a rotating impeller is described and the results of a calculation presented. An experimental facility is described to examine the pressure and velocity distribution in a rotating cascade with either inflow or outflow. The results are given for a straight-vaned, constant area, impeller operating under radial inflow turbine conditions. The experimental results show that the general trends of the relative velocity and static pressure distribution in the rotor predicted by the potential theory were observed. The differences between experiment and theory could be accounted for by friction effects in the passage associated with boundary-layer growth and turbulence.

ACKNOWLEDGMENTS

The authors wish to acknowledge, with thanks, help received from the Science Research Council, D. Napier & Son Ltd., C.A.V. Ltd., the National Gas Turbine Establishment, and the Worthington Corporation for financial support in the radial turbomachinery research programs pursued at the University of Manchester Institute of Science and Technology for the past five years.

The authors wish to thank D. C. Jackson and K. Herath, and all those associated with the research program.

REFERENCES

1 Benson, R. S., "An Analysis of the Losses in a Radial Gas Turbine," Proceedings of

the Institute of Mechanical Engineers, Vol. 180, Part 3J, 1965-1966, pp. 41-53.

2 Benson, R. S., Cartwright, W. G., and Das, S. K., "Turbine at Zero Incidence," Proceedings of the Institute of Mechanical Engineers, Vol. 182, Part 3H, 1967-1968, pp. 211-231.

3 Benson, R. S., and Barnard, M. C. S., "Radial Gas Turbines," Proceedings of the Institute of Mechanical Engineers, Vol. 183, Part 3N, 1968-1969.

4 Benson, R. S., Cartwright, W. G., and Woollatt, G., "Calculations of the Flow Distribution within a Radial Turbine Rotor," Institute of Mechanical Engineers, Thermodynamics and Fluid Mechanics Convention, Paper No. 8, 1970.

5 Benson, R. S., Cartwright, W. G., and Jackson, D. C., "Flow Studies in a Low Speed Radial Bladed Impeller," Institute of Mechanical Engineers, Thermodynamics and Fluid Mechanics Convention, Paper No. 15, 1970.

6 Benson, R. S., "A Review of Methods for Assessing Loss Coefficients in Radial Gas Turbines," to be published in IJMS.

7 Benson, R. S., "Prediction of Performance of Radial Gas Turbines in Automotive Turbochargers," to be presented at 1971 Houston ASME Gas Turbine Conference.

8 Katsanis, T., "Use of Arbitrary Quasi-Orthogonals for Calculating Flow Distribution in the Meridional Plane of a Turbomachine," NASA Technical Note D-2546, 1964.

9 Katsanis, T., "Use of Arbitrary Quasi-Orthogonals for Calculating Flow Distribution on a Blade to Blade Surface in a Turbomachine," NASA Technical Note D-2809, 1965.

10 Katsanis, T., "Fortran Program for Calculating Transonic Velocities on a Blade-to-Blade Stream Surface of a Turbomachine," NASA Technical Note 5427, Sept. 1969.

11 Stanitz, J. D., "Some Theoretical Aerodynamic Investigations of Impellers in Radial and Mixed-Flow Centrifugal Compressors," Transactions ASME, Vol. 74, 1952, p. 473.

12 Ames, W. F., "Numerical Methods for Partial Differential Equations," (Nelson), 1969.

13 Young, G. A. J., "The Flow in the Rotating Passages of a Centrifugal Pump Impeller," BHRA Publication No. SP 530, April 1956.

14 Simpson, H. C., and Cinnamond, D. C., "Studies of Flow Through Centrifugal Pump Impellers," Proceedings of the Institute of Mechanical Engineers, Vol. 178, Part 3I (ii), 1963-1964, p. 43.

15 Acosta, A. J., and Bowerman, R. D., "An Experimental Study of Centrifugal Pump Impellers," Transactions of the ASME, Vol. 79, Nov. 1957, p. 1821.

16 Cartwright, W. G., and Hill, M. J., "The Calculation of Two-Dimensional Flows in Radial Turbomachines," in preparation for publication.